



# Mechanical integrity of corrosion product films on rotating cylinder specimens



L.D. Paolinelli <sup>a,\*</sup>, G.E. Carr <sup>b</sup>

<sup>a</sup> Institute for Corrosion and Multiphase Technology, Ohio University, Athens, OH 45701, USA

<sup>b</sup> INTEMA, CONICET, National University of Mar del Plata, J.B. Justo 4302, 7600 Mar del Plata, Argentina

## ARTICLE INFO

### Article history:

Received 7 July 2014

Accepted 27 November 2014

Available online 5 December 2014

### Keywords:

B. Modelling studies

C. Effects of strain

C. Interfaces

## ABSTRACT

Rotating cylinder (RC) technique is widely used for flow corrosion testing. However, this test configuration has limitations. Particularly, integrity of corrosion products films formed on the RC surface can be affected. The objective of this work is to show how intense the stresses in corrosion product films can be at high rotation speeds. In such cases, failure of the films is possible due to inertial forces rather than other factors, such as flow, leading to erroneous results. Consequently, theoretical calculation of stresses in films has been performed and a case of corrosion product film failure assessed using a fracture mechanics approach.

© 2014 Elsevier Ltd. All rights reserved.

## 1. Introduction

The rotating cylinder (RC) technique has been widely used in corrosion laboratory testing to determine the effect of flow velocity on corrosion rates [1–8]. The obtained information can be used to predict the corrosion behavior of the internal walls of pipes in industrial applications. This is usually achieved by using characteristic flow-related parameters such as the mass transfer coefficient, for which formulations for RC configuration are available elsewhere [5,6]. However, this test configuration is not exempt from complications. Particularly, the rotation-induced inertial forces acting on the whole volume of the RC can play an important role on the integrity of solid corrosion products or deposits that may form on the RC surface.

The objective of this paper is to show that the stresses in RC corrosion product films can be significant, particularly when high rotation speeds are employed. Under these conditions unnatural failure of corrosion product films may be possible due to inertial forces rather than other well-known factors under study, such as flow, which leads to erroneous conclusions.

Regarding this matter, a theoretical approach to the calculation of the stress field of corrosion product films is introduced. Moreover, an experimental case of film failure is assessed using available fracture mechanics knowledge. The results indicate that

under certain experimental conditions the use of the RC technique can provoke spontaneous fracture of the corrosion product film, which is undesired in the corrosion test.

### 1.1. Stresses in corrosion product films attached on the cylindrical external surface of a RC

Uniform corrosion product layers attached on a metallic surface can be modeled as thin films. If a uniform isotropic elastic film of thickness  $h$  is completely adhered on the cylindrical external surface of a RC (Fig. 1), it can be presumed that the attached surface of the film will share the same displacement field as the substrate surface (attachment boundary condition). This is expressed as the equality of the strains of the film and the strains of the substrate surface in the tangential ( $t$ ) and the axial ( $z$ ) directions:

$$\varepsilon_{tf} = \varepsilon_{ts} \quad (1)$$

$$\varepsilon_{zf} = \varepsilon_{zs} \quad (2)$$

The subscripts  $f$  and  $s$  indicate whether the strain corresponds to the film or the substrate surface, respectively.

As the film is considered to be very thin, its radial stress component can be neglected ( $\sigma_{rf} \sim 0$ ). Moreover, the constraint that the adhered film could cause on the substrate is also ignored; this means that if the substrate is loaded in some way it will respond as if nothing is on its surface.

If the cylinder length is larger than its diameter and the cylinder is unloaded in the axial direction, the axial strain of the substrate

\* Corresponding author at: Institute for Corrosion and Multiphase Technology, Department of Chemical and Biomolecular Engineering, Ohio University, 342W. State Street, Athens, OH 45701, USA. Tel.: +1 740 593 0283; fax: +1 740 593 9949.

E-mail address: [paolinel@ohio.edu](mailto:paolinel@ohio.edu) (L.D. Paolinelli).

### Nomenclature list

$a$	half of the length of a preexisting characteristic defect in the corrosion product film	$\nu_s$	Poisson's ratio of the substrate
$\alpha_f$	thermal expansion coefficient of the film	$P$	porosity of the film material
$\alpha_s$	thermal expansion coefficient of the substrate	$R_1$	inner radius of the RC
$\alpha$	Dundurs parameters	$R_2$	outer radius of the RC
$\beta$		$Re$	Reynolds number
$\Delta T$	temperature variation	$\rho_s$	density of the RC material
$E_f$	Young's modulus of the film	$\rho_n$	density of the fluid around the RC
$E_o$	Young's modulus of the pore-free material of the film	$\sigma_{ij}$	stress tensor
$E_s$	Young's modulus of the substrate	$\sigma_{rf}$	radial normal stress component in the film
$\epsilon_{tf}$	tangential strain in the film	$\sigma_{rs}$	radial normal stress component in the substrate
$\epsilon_{ts}$	tangential strain in the substrate	$\sigma_{rr}$	radial normal stress component in the corrosion product film of $\text{FeCO}_3$
$\epsilon_{zf}$	axial strain in the film	$\sigma_{rt}$	shear stress component in the corrosion product film of $\text{FeCO}_3$ (acting in tangential direction)
$\epsilon_{zs}$	axial strain in the substrate	$\sigma_{tf}$	tangential normal stress component in the film
$f$	friction factor	$\sigma_{ts}$	tangential normal stress component in the substrate
$f(a/l, \nu_f)$	dimensionless function of $a/l$ and $\nu_f$ estimated by means of numerical methods	$\sigma_{tt}$	tangential normal stress component in the corrosion product film of $\text{FeCO}_3$
$g(\alpha, \beta)$	dimensionless function dependent on the Dundurs parameters	$\sigma_{zf}$	axial normal stress component in the film
$h$	film thickness	$\sigma_{zs}$	axial normal stress component in the substrate
$K_C$	critical stress intensity factor	$\sigma_{zz}$	axial normal stress component in the corrosion product film of $\text{FeCO}_3$
$K_{IC}$	critical mode I stress intensity factor	$\sigma_t$	thermal stress in the film
$K_I$	mode I stress intensity factor	$\tau_w$	wall shear stress
$K_o$	bulk modulus of the pore-free material of the film	$U$	velocity at the surface of the RC
$l$	reference length	$\mu_n$	dynamic viscosity of the fluid around the RC
$\nu_f$	Poisson's ratio of the film	$\omega$	rotation speed
$\nu_o$	Poisson's ratio of the pore-free material of the film		

can be ignored ( $\epsilon_{zs} = 0$  and  $\sigma_{zs} \neq 0$ ). The radial stress component of the surface substrate ( $\sigma_{rs}$ ) is considered as zero.

Using Hooke's law (strain–stress relationship) to relate the strains in the film and in the substrate with their respective stresses, the Eqs. (1) and (2) can be written as:

$$\frac{\sigma_{ts} - \nu_s \sigma_{zs}}{E_s} = \frac{\sigma_{tf} - \nu_f \sigma_{zf}}{E_f} \quad (3)$$

$$\frac{\sigma_{zs} - \nu_s \sigma_{ts}}{E_s} = \frac{\sigma_{zf} - \nu_f \sigma_{tf}}{E_f} = 0 \quad (4)$$

where  $E_f$  and  $E_s$  are Young's moduli of the film and the substrate, respectively;  $\nu_f$  and  $\nu_s$  are Poisson's ratios of the film and the substrate, respectively;  $\sigma_{rf}$ ,  $\sigma_{tf}$  and  $\sigma_{zf}$  are the radial, tangential and axial normal stresses in the film, respectively;  $\sigma_{rs}$ ,  $\sigma_{ts}$  and  $\sigma_{zs}$  are the radial, tangential and axial normal stresses in the substrate surface, respectively.

Combining Eqs. (3) and (4), the tangential and the axial stresses in the film can be expressed as a function of the surface tangential stress of the substrate:

$$\sigma_{tf} = \sigma_{ts} \frac{(1 - \nu_s^2) E_f}{(1 - \nu_f^2) E_s} \quad (5)$$

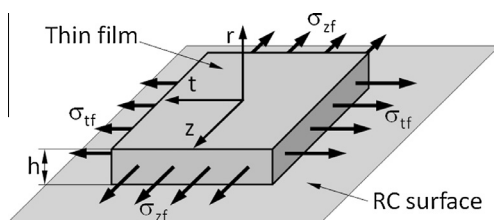


Fig. 1. Schematic of a portion of a uniform thin film attached on the RC surface.

$$\sigma_{zf} = \sigma_{ts} \frac{\nu_f (1 - \nu_s^2) E_f}{(1 - \nu_f^2) E_s} \quad (6)$$

From Eqs. (5) and (6) the stresses in the film have a linear dependence on the tangential stress of the substrate surface ( $\sigma_{ts}$ ). The main factor that controls the stress transferred from the substrate to the film is the quotient between Young's moduli of the film and the substrate materials ( $E_f/E_s$ ).

#### 1.1.1. Rotation-induced stresses

Rotating solid bodies develop internal stresses in order to equilibrate the volume forces produced by the resulting accelerations. In the case of a RC apparatus, the working piece or electrode can be modeled as a rotating hollow cylinder made of an isotropic elastic material.

If the RC rotates at constant speed ( $\omega$ ) around its symmetry axis (named here  $z$ ), the developed internal stresses will be: radial stress ( $\sigma_r$ ), tangential stress ( $\sigma_t$ ), and axial stress ( $\sigma_z$ ). These stresses are present through the section of the RC and vary with the radius [9].

Consequently, if a thin film is adhered or deposited on the cylindrical external surface of a stationary RC and subsequently the RC is rotated at a constant speed ( $\omega$ ), it will experience normal stresses in the tangential and the axial directions due to the strains in the substrate. According to Eqs. (5) and (6), the tangential stress at the RC surface will be needed to calculate the stresses in the adhered film. From integrating differential equations (Hooke's law and force balance) and applying boundary conditions ( $\sigma_{rs}(R_1) = \sigma_{rs}(R_2) = 0$ ; surfaces are unloaded in the radial direction at  $R_1$  and  $R_2$ , internal and external radii of the hollow cylinder, respectively), the tangential stress at the RC surface results [9]:

$$\sigma_{ts} = \frac{\rho_s \omega^2}{4(1 - \nu_s)} [(3 - 2\nu_s) R_1^2 + (1 - 2\nu_s) R_2^2] \quad (7)$$

where  $\rho_s$  is the density of the cylinder material.

Replacing the tangential stress ( $\sigma_{ts}$ ) in Eqs. (5) and (6) by Eq. (7), the tangential and the axial stresses in the film can be calculated as a function of the rotation speed and geometry of the RC:

$$\sigma_{tf} = \frac{\rho_s \omega^2}{4(1 - \nu_s)} \left[ (3 - 2\nu_s)R_1^2 + (1 - 2\nu_s)R_2^2 \right] \frac{(1 - \nu_s^2)E_f}{(1 - \nu_f^2)E_s} \quad (8)$$

$$\sigma_{zf} = \frac{\rho_s \omega^2}{4(1 - \nu_s)} \left[ (3 - 2\nu_s)R_1^2 + (1 - 2\nu_s)R_2^2 \right] \frac{\nu_f(1 - \nu_s^2)E_f}{(1 - \nu_f^2)E_s} \quad (9)$$

The expressions above indicate that both the tangential and the axial stresses in the film will be tensile if the film is adhered in stationary or quasi-stationary conditions and then rotated. Eqs. (8) and (9) can also be used to estimate the stresses in a film that is adhered under a constant rotation speed and then the rotation is stopped, but in that case the generated stresses will be compressive.

### 1.1.2. Flow-induced stresses

The RC apparatus is commonly employed to provide the cylindrical external area of the working electrode with hydrodynamic conditions comparable to those experienced on the internal walls of pipes during industrial operation. One of the parameters of interest to be matched in many cases is the wall shear stress. The mean wall shear stress on a RC smooth surface can be estimated with the following equation:

$$\tau_w = \frac{1}{2} f \rho_f U^2 \quad (10)$$

where  $f$  is the friction factor,  $\rho_f$  is the density of the fluid, and  $U$  is the velocity at the cylinder surface ( $U = \omega R_2$ ).

The friction factor can be related to the Reynolds number as follows [10] ( $1000 \leq Re \leq 100,000$ ):

$$\frac{f}{2} = 0.0791 Re^{-0.3} \quad (11)$$

The Reynolds number is based on the diameter of the cylinder:  $Re = 2\rho_f R_2 U / \mu_f$ , where  $\mu_f$  is the dynamic viscosity of the fluid. In general the RC is used in turbulent flow when  $Re > 200$  [11].

Numerical studies on the turbulent flow field of a RC indicate that the fluctuations of the mean wall shear stress value ( $\tau_w$ , defined by Eqs. (10) and (11)), expressed in terms of rms (root mean square), can be around 0.3 (30%). Moreover, the peak values of wall shear stress can rise up to twice its mean value [12]. It must also be taken into account that the average wall pressure fluctuations (rms variation of the surface stress in the normal direction) can be as high as 1.3 and 2 times the mean wall shear stress for  $Re$  numbers of approximately 3600 and 18,000, respectively [12]. The fluctuating wall shear stresses as well as the fluctuating wall normal stresses and their frequencies may be important when assessing the structural integrity of a corrosion product film.

### 1.1.3. Thermally-induced stresses

If temperature changes are experienced after forming the film on the substrate, the thermally-induced stresses must also be taken into account, mainly when the thermal expansion coefficients of the film and the substrate are different. The thermal stresses in the film can be estimated as follows:

$$\sigma^t = E_f \frac{(\alpha_s - \alpha_f)\Delta T}{(1 - \nu_f)} \quad (12)$$

where  $\alpha_f$  and  $\alpha_s$  are the thermal expansion coefficients of the film and the substrate, respectively; and  $\Delta T$  is the temperature variation.

### 1.1.4. Total stress field

If an intrinsic or residual stress field, or other type of stress field (e.g. flow-induced, Section 1.1.2) is present in the corrosion product film, it must be added to the stress components calculated by Eqs (8) and (9) (Section 1.1.1) in order to determine the total stress state in the film.

### 1.1.5. Mechanical properties of the corrosion product films

From the previous sections it is clear that to perform a theoretical assessment of the internal stresses in a corrosion product film, its mechanical properties have to be known a priori. In general, corrosion product films are porous structures which can present diverse microstructures and compositions. Here, models to account for the mechanical properties of porous materials are introduced. Young's modulus and Poisson's ratio can be modeled as [13]:

$$E_f = E_o(1 - P^{2/3})^{1.21} \quad (13)$$

$$\nu_f = 0.5 - \frac{(1 - P^{2/3})^{1.21} [2(3 - 5P)(1 - 2\nu_o) + 3P(1 + \nu_o)]}{4(3 - 5P)(1 - P)} \quad (14)$$

where  $P$  is the volume fraction of porosity, and  $E_o$  and  $\nu_o$  are Young's modulus and Poisson's ratio of the pore-free material, respectively.

Although Eqs. (13) and (14) were developed for spherical pore geometry, they have been used to obtain good agreement with experimental data for materials with varied pore structures and low porosities ( $P < 0.5$ ).

## 1.2. Failure of corrosion product films during RC tests

### 1.2.1. Case study

In previous work by Ruzic et al. [2–4], protective iron carbonate ( $\text{FeCO}_3$ ) corrosion product films were developed on a carbon steel RC at low rotation speed (200 rpm) in a glass cell with  $\text{CO}_2$ -containing brine at 80 °C. Once these protective iron carbonate films were well developed, the RC speed was increased to a range of 7000–10,000 rpm in order to study the effect of the flow-induced wall shear stresses on their integrity. After increasing the RC speed, it was found that corrosion product films consistently fractured in the axial direction at several surface locations. Fig. 2 shows a back scatter SEM image of the surface topography of a characteristic  $\text{FeCO}_3$  film previously formed at low rotation rate (200 rpm) and subsequently tested at a speed of 7000 rpm for 2.5 h. The  $\text{FeCO}_3$  film shows through-thickness cracks oriented in the axial direction, called 'vertical cracks' by Ruzic et al., which can reach more than 1 mm in length. This failure was detected indirectly by *in situ* electrochemical measurements of the corrosion rate of the carbon

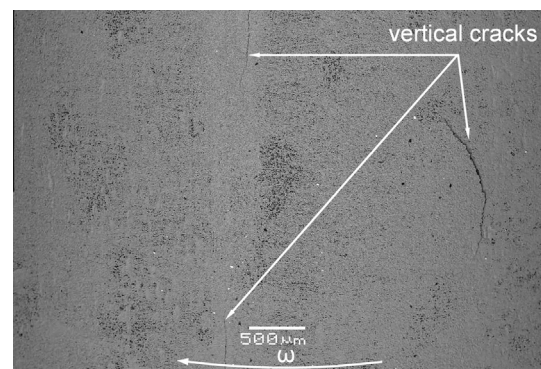


Fig. 2. Typical surface topography (BSE) of an  $\text{FeCO}_3$  film formed at low rotation rate (200 rpm) and subsequently rotated at 7000 rpm for 2.5 h. Picture is courtesy of Prof. Srdjan Nestic.

steel substrate, which progressively increased after the cracking occurred since the electrolyte came in contact with the bare steel surface. After long exposure times at high rotation speed, detachment of portions of the film was observed.

The authors commented about the possible influence of centrifugal forces on the failure of the corrosion product films; however, they did not make any quantification of this effect. Moreover, it was discussed that the main mechanical factor involved in the failure of the films was the flow-induced fluctuating stresses on the RC surface.

It must be mentioned that the thermal residual stresses, which the film may experience because of the cooling down of the RC samples from 80 °C to room temperature when extracted from the glass cell, were not responsible for the film cracking since failures were not found in films rotated at low speed (200 rpm). Thermal residual stresses are not expected when varying the temperature of the samples since the thermal expansion coefficients of the iron carbonate ( $\sim 1.26 \times 10^{-5} \text{ }^\circ\text{C}^{-1}$  [14,15]) and carbon steel ( $\sim 1.2 \times 10^{-5} \text{ }^\circ\text{C}^{-1}$  [16]) are similar.

During the remainder of this work, theoretical calculations of the internal stress field of a rotated  $\text{FeCO}_3$  corrosion product film of similar characteristics to the ones tested in previous research [2–4] will be performed using the equations introduced above and taking into consideration the effect of film porosity. In addition, the film failure will be assessed using a fracture mechanics approach.

### 1.2.2. Fracture mechanics analysis

As will be shown later, there is a large tensile stress component in the tangential direction due to the rotation of the RC affecting the iron carbonate films described in the previous section. In order to determine if such a stress component can be responsible for the occurrence of the axial cracks in the iron carbonate film (Fig. 2), a fracture mechanics analysis is performed. The driving force for the propagation of axial through-thickness or ‘channeling’ cracks from a preexisting defect in the film (Fig. 3) is calculated in the form of stress intensity factor ( $K$ ), taking into account the film/substrate attachment, the elastic mismatch between the film and the substrate, and the thickness of the film. The curvature of the RC surface is neglected treating the film/substrate interface as plane. Moreover, the only contribution for the through-thickness crack propagation is mode I ( $K_I \neq 0$ ) driven by the uniform tensile stress,  $\sigma_{tt}$ . The shear stress in the axial direction ( $\sigma_{tz}$ ) is zero ( $K_{II} = 0$ ), and the shear stress in the radial direction ( $\sigma_{tr} = \sigma_{rt} \sim 0$ ) is neglected ( $K_{III} = 0$ ). Thus, the stress intensity factor at the crack tip can be calculated as follows [17]:

$$K_I = f(a/l, \nu_f) \sigma_{tt} \sqrt{l} \quad (15)$$

where  $f(a/l, \nu_f)$  is a dimensionless function of  $a/l$  and  $\nu_f$ , estimated by means of numerical methods;  $\sigma_{tt}$  is the known tensile tangential stress applied normal to the crack direction,  $a$  is the half-length of

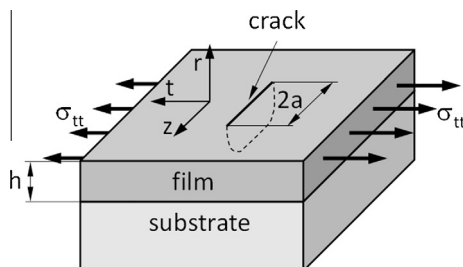


Fig. 3. Schematic of a portion of film attached on the RC substrate and loaded with tensile stress, showing a through-thickness finite crack of length  $2a$ .

a preexisting defect or crack in the film, and  $l$  is the reference length which is defined as:

$$l = \frac{\pi}{2} g(\alpha, \beta) h \quad (16)$$

where  $h$  is the thickness of the film and  $g(\alpha, \beta)$  is a dimensionless function that depends on the Dundurs parameters,  $\alpha$  and  $\beta$ , which characterize the elastic mismatch between the film and the substrate:

$$\alpha = \frac{\bar{E}_f - \bar{E}_s}{\bar{E}_f + \bar{E}_s} \quad (17)$$

$$\beta = \frac{1}{2} \frac{\mu_f(1 - 2\nu_s) - \mu_s(1 - 2\nu_f)}{\mu_f(1 - \nu_s) + \mu_s(1 - \nu_f)} \quad (18)$$

where  $\mu = E/(2(1 + \nu))$  is the shear modulus and  $\bar{E} = E/(1 - \nu^2)$  is a plane strain tensile modulus where the subscripts  $f$  and  $s$  refer to the film and the substrate, respectively.

## 2. Materials and methods

### 2.1. Characterization of the corrosion product films of $\text{FeCO}_3$ obtained in RC tests

The formation and testing of the corrosion product films were done using a RC apparatus in a glass cell. Specific information about the performed experiments (solution chemistry, procedure for corrosion product film formation, etc.) can be found in Ruzic's research [2].

Fig. 4 shows SEM images of the surface topography and the cross section of a characteristic  $\text{FeCO}_3$  film formed at 200 rpm. It is observed that the iron carbonate film developed on the steel surface has uniform thickness of about 50  $\mu\text{m}$  and presents a smooth topography. It can also be seen from the cross-sections that the distribution and shape of the pores in the film are not uniform, showing zones with large pores somewhat aligned parallel to the RC surface, and compact zones with small pores. From image analysis of cross-sections it was determined that the overall porosity of these films does not exceed 0.3 (30%). The theoretical mechanical assessment of these films will be performed for several porosity levels (from 0.1 to 0.4) to account for the uncertainty in the determination of this parameter.

### 2.2. Parameters used for the mechanical assessment of the $\text{FeCO}_3$ films

#### 2.2.1. Mechanical properties of $\text{FeCO}_3$

Young's modulus of the pore-free iron carbonate obtained from theoretical molecular calculation will be 134 GPa [18]. Poisson's ratio of the pore-free  $\text{FeCO}_3$  can be obtained using the following known relationship:

$$\nu_o = \frac{1}{2} \left( 1 - \frac{E_o}{3K_o} \right) \quad (19)$$

where  $K_o$  is the bulk modulus of the pore-free iron carbonate, which is assumed to be 114 GPa [18]. Thus, according to Eq. (19), the Poisson ratio value of the pore-free iron carbonate is 0.304.

#### 2.2.2. Calculation of the stress field in the corrosion product film of $\text{FeCO}_3$

To model the problem described in Section 1.2.1, a thin porous film of  $\text{FeCO}_3$  with similar characteristics to the one shown in Section 2.1 (uniform thickness of 50  $\mu\text{m}$  and smooth surface) is presumed to be completely adhered on the external cylindrical surface of the RC. The film is supposed to be unstressed ( $\sigma_{ij} = 0$ )

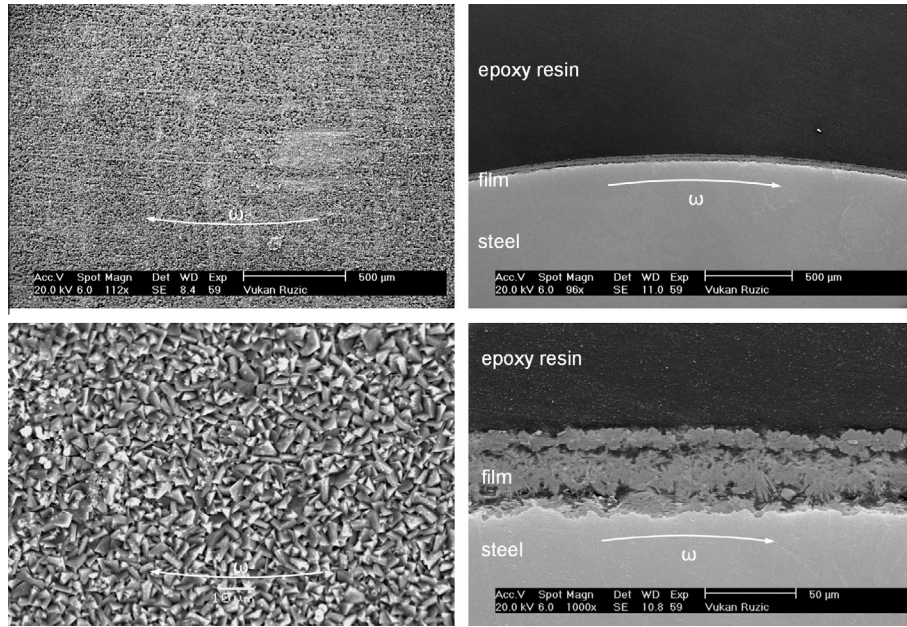


**Fig. 4.** Typical surface topography (left) and cross-section (right) of an  $\text{FeCO}_3$  film on the steel surface at the end of the formation process at 200 rpm. Pictures are courtesy of Prof. Srdjan Nestic.

for a rotation speed ( $\omega$ ) of 200 rpm; thus, intrinsic or residual stresses are not considered.

Eqs. (8) and (9) are used to estimate the rotation-induced  $\sigma_{rt}$  (tangential) and  $\sigma_{zz}$  (axial) normal stress components, respectively. The shear stress component ( $\sigma_{rt}$ ) exerted by the fluid flow are calculated using Eq. (10). The subscripts of the stress components refer to the axis system ( $rtz$ ) shown in Fig. 1 where  $r$ ,  $t$ , and  $z$  are the radial, tangential, and axial directions, respectively.

The properties of the RC material (carbon steel) used for the stress calculations are density ( $\rho_s$ ) 7800 kg/m<sup>3</sup>, Young’s modulus ( $E_s$ ) 210 GPa, and Poisson’s ratio ( $\nu_s$ ) 0.3. The properties of the fluid moving around the RC (aqueous brine at 80 °C) are density ( $\rho_f$ ) 972 kg/m<sup>3</sup> and dynamic viscosity ( $\mu_f$ ) 3.57.10<sup>-4</sup> Pa s. The RC inner and outer diameters adopted for the calculations are 6.5 mm ( $2R_1$ ) and 12 mm ( $2R_2$ ), respectively.

### 3. Results and discussion

#### 3.1. Stress field in corrosion product films of $\text{FeCO}_3$ under rotation

Fig. 5 shows the estimated values of the stress components in a thin  $\text{FeCO}_3$  film with a porosity of 0.3 (30%) as a function of the rotation rate. All of the stress components increase with rotation rate. Moreover, the normal stresses ( $\sigma_{rt}$ , acting in the tangential direction, and  $\sigma_{zz}$ , acting in the axial direction) are several orders of magnitude higher than the shear stress ( $\sigma_{rt}$ , acting in the tangential direction). Even if wall shear stress fluctuations and pressure fluctuations (additional normal stress component acting in the radial direction,  $\sigma_{rr}$ ) due to the turbulent RC flow are considered in the total stress state characterization of the film, their relative contribution is negligible. These results indicate that the

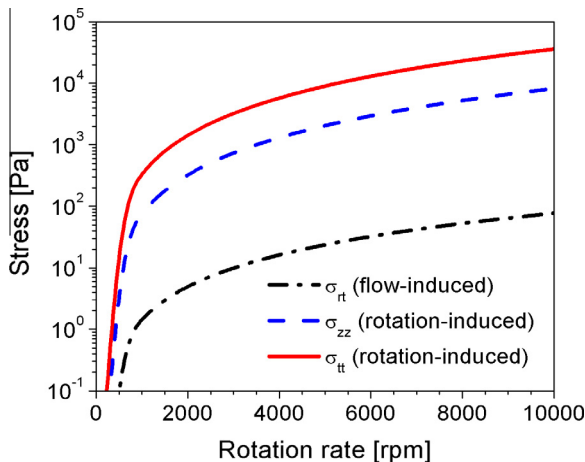


**Fig. 5.** Calculated stress components in a porous thin film of  $\text{FeCO}_3$  adhered to the RC surface as a function of rotation rate (film porosity: 0.3, RC material: carbon steel, RC inner diameter: 6.5 mm, RC outer diameter: 12 mm, fluid: aqueous brine, temperature: 80 °C).

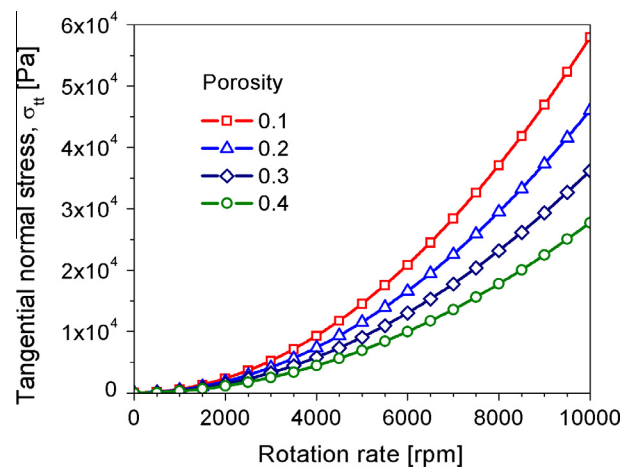


**Fig. 6.** Calculated tangential normal stress in thin  $\text{FeCO}_3$  films with different porosities adhered to the RC surface as a function of rotation rate (RC material: carbon steel, RC inner diameter: 6.5 mm, RC outer diameter: 12 mm).

main stresses in the film are produced by the RC rotation rather than the turbulent flow.

Regarding the main stress components in the film, the axial normal stress ( $\sigma_{zz}$ ) can be about 10–30% of the value of the tangential normal stress ( $\sigma_{tt}$ ) depending on the value of the Poisson ratio of the film.

Fig. 6 shows that increasing the porosity decreases the tangential normal stress ( $\sigma_{tt}$ ). Despite the drop in the normal stress values with increasing porosity, the rotation-induced stress components always have a greater impact than the stress components produced by the turbulent flow around the RC.

From the stress analysis performed, a mechanical failure such as that seen in Fig. 2 (cracks oriented in the axial direction of the RC) is no longer unexpected since the largest tensile stress component found in the film is acting in the tangential direction ( $\sigma_{tt}$ ).

### 3.2. Stress intensity factors for defective films of $\text{FeCO}_3$ under rotation

Fig. 7 shows the calculated values of stress intensity factors for different pre-existing defect or crack lengths in an  $\text{FeCO}_3$  film of 50  $\mu\text{m}$  thickness with different porosities attached on the surface of the RC rotating at 7000 rpm. The defect lengths ( $2a$ ) considered for the calculation of the stress intensity factors range from less than an  $\text{FeCO}_3$  average grain size ( $\sim 3\text{--}7\ \mu\text{m}$ , Fig. 4) to a distance equivalent to the film thickness (50  $\mu\text{m}$ ). However, defects with sizes larger than the film thickness may also exist due to the non-uniform conformation of the corrosion product layer (Fig. 4, cross-section).

It is interesting to note that the variation of the stress intensity factor with the porosity of the film is not proportional. This result is non-trivial and is related to the complicated nature of the stress intensity factor function (Eq. (15)). For example, porosities of 0.1 and 0.2 show similar stress intensity factor values for all the evaluated range of defect sizes. On the other hand, increasing porosity from 0.2 to 0.3 reduces the stress intensity factor approximately 40% for almost all of the assessed defect lengths. It can be anticipated from Eqs. (15) and (16) that the stress intensity factor will increase with film thickness.

It is supposed that if failure of the film occurs it will be brittle, with negligible energy consumption in plastic work around the crack tip as observed in most ceramic materials. Hence, the crack growth from an existing defect will occur spontaneously when the required energy level, defined in terms of stress intensity factor, reaches the critical value  $K_{IC}$ . The  $K_{IC}$  value is an intrinsic property of the material that is determined experimentally.

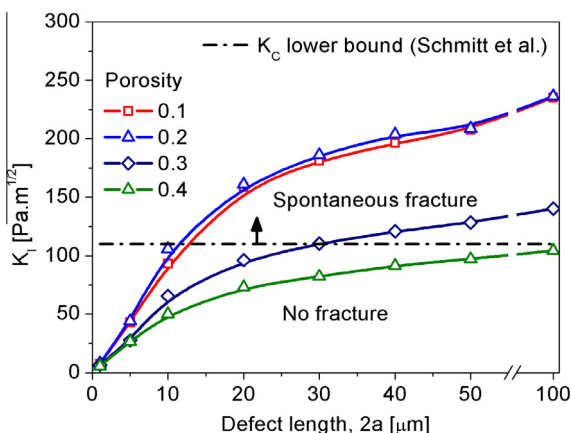


Fig. 7. Stress intensity factor values for different pre-existing defect lengths in an  $\text{FeCO}_3$  film of 50  $\mu\text{m}$  thickness with different porosities attached on a RC surface at 7000 rpm (RC material: carbon steel, RC inner diameter: 6.5 mm, RC outer diameter: 12 mm).

The values of  $K_{IC}$  for corrosion product films of  $\text{FeCO}_3$  formed on carbon steel surfaces are not easy to determine due to the micro-inhomogeneity of their structures (polycrystalline single or multi-layer structure, porosity, non-uniform flow distribution, and the presence of non-corroded carbide residues, among other factors). Moreover, the information available in the literature regarding  $K_{IC}$  values for the inter- and/or intra-granular brittle fracture of iron carbonate films is scarce and inconsistent [19–23]. Despite this fact, there are some useful data to analyze.

Schmitt, et al. [20] measured  $K_{IC}$  values from 110 to 360 Pa m<sup>1/2</sup> for iron carbonate films that had comparable characteristics and were formed under similar conditions (temperature: 80 °C, flow velocity: 2 m/s,  $P_{\text{CO}_2}$ : 0.5 MPa) to those of the films under evaluation. When the reported  $K_{IC}$  values are compared to the calculated  $K_{IC}$  values for different defect lengths shown in Fig. 7, it is found that spontaneous fracture can occur in films with porosities of 0.1–0.2 with a defect length as small as 10  $\mu\text{m}$ . Moreover, for a considerable porosity level such as 0.3, the critical defect size to trigger the failure can be as small as 30  $\mu\text{m}$ . This analysis would justify the occurrence of the relatively long axial cracks seen in Fig. 2 and previous work [2,3].

It is worth noting that the cracks propagated in the axial direction while rotating the RC at high speed finally arrest (Fig. 2). This behavior could be related to a film/substrate interface debonding and/or interface debonding in between film layers (parallel to the substrate) which can modify the stress intensity to continue propagating the crack as was discussed elsewhere [24]. Additionally, if a propagating crack induces an interface debonding on one side of the crack but not the other, it produces a strong asymmetry with respect to the crack tip causing the crack to follow a curved trajectory [17], which can be observed for one of the cracks shown in Fig. 2.

The intrinsic or residual stresses of the  $\text{FeCO}_3$  films formed in the RC tests in [2,3] (Figs. 2 and 4) should not be too significant since the mechanical assessment performed without considering their effect is in good agreement with the experimental results.

It is clear that RC corrosion tests involving the formation of corrosion product films need to be carefully designed based not only on parameters such as wall shear stresses or mass transfer coefficients but also on the mechanical integrity of the formed corrosion product films. The assessments introduced in this paper can be applied to different RC materials and corrosion product films as well as deposited scales, if their mechanical properties and film or scale thickness are known.

## 4. Conclusions

Theoretical formulations were introduced for the calculation of the rotation-induced stress field of corrosion product films adhered to RC substrates as a function of the rotation speed and the film and substrate's elastic properties (Young's modulus and Poisson's ratio). The quantification of these stresses as well as the flow-induced and residual (intrinsic and thermal) stresses elucidates the actual stress state of the corrosion product films for their mechanical assessment.

Under particular experimental conditions the use of RC in corrosion tests can be harmful for the mechanical integrity of the formed corrosion product films. This concern is especially important if the formed films have brittle fracture behavior. In this work, it has been demonstrated by means of mechanical assessment that  $\text{FeCO}_3$  corrosion product films formed on RC carbon steel substrates at low rotation rates can be fractured when rotated at higher speeds due to the high inertial tensile stresses produced. This type of unnatural failure can cause misleading corrosion results.

Therefore, RC corrosion tests involving the formation of corrosion product films need to be carefully designed based not only on parameters such as wall shear stresses or mass transfer coefficients but also on the mechanical integrity of the formed corrosion product films.

### Acknowledgments

The authors want to acknowledge Prof. Srdjan Nestic for providing valuable experimental data and technical discussion, as well as Dr. Bruce Brown for his valuable comments and support. This work was funded by the Institute for Corrosion and Multiphase Technology.

### References

- [1] S. Nestic, J. Postlethwaite, S. Olsen, An electrochemical model for prediction of corrosion of mild steel in aqueous carbon dioxide solutions, *Corrosion* 52 (1996) 280–294.
- [2] V. Ruzic, M. Veidt, S. Nešić, Protective iron carbonate films—Part 1: Mechanical removal in single-phase aqueous flow, *Corrosion* 62 (2006) 419–432.
- [3] V. Ruzic, M. Veidt, S. Nešić, Protective iron carbonate films—Part 3: Simultaneous chemo-mechanical removal in single-phase aqueous flow, *Corrosion* 63 (2007) 758–769.
- [4] V. Ruzic, M. Veidt, S. Nešić, Protective iron carbonate films—Part 2: Chemical removal by dissolution in single-phase aqueous flow, *Corrosion* 62 (2006) 598–611.
- [5] D.C. Silverman, Rotating cylinder electrode for velocity sensitivity testing, *Corrosion* 40 (1984) 220–226.
- [6] D.C. Silverman, Rotating cylinder electrode – geometry relationships for prediction of velocity-sensitive corrosion, *Corrosion* 44 (1988) 42–49.
- [7] S. Nestic, G.T. Solvi, S. Skjerve, Comparison of rotation cylinder and loop methods for testing CO<sub>2</sub> corrosion inhibitors, *Br. Corros. J.* 32 (1997) 269–276.
- [8] L.D. Paolinelli, B. Brown, S.N. Simison, S. Nestic, Inhibition of CO<sub>2</sub> corrosion of carbon steel with 1% Cr, *Mater. Chem. Phys.* 136 (2012) 1092–1102.
- [9] E.J. Hearn, Rings, discs and cylinders subjected to rotation and thermal gradients, in: *Mechanics of Materials—An Introduction to the Mechanics of Elastic and Plastic Deformation of Solids and Structural Material*, Elsevier, Amsterdam, 1997, pp. 117–129.
- [10] M. Eisenberg, C.W. Tobias, C.R. Wilke, Ionic mass transfer and concentration polarization at rotating electrodes, *J. Electrochem. Soc.* 101 (1954) 306–320.
- [11] T. Theodorsen, A. Regier, Experiments on drag of revolving disks, cylinders and streamline rods at high speeds, in: *National Advisory Committee for Aeronautics*, Langley Field, Va, 1944.
- [12] J.-Y. Hwang, K.-S. Yang, D.-H. Yoon, K. Bremhorst, Flow field characterization of a rotating cylinder, *Int. J. Heat Fluid Flow* 29 (2008) 1268–1278.
- [13] M. Arnold, A.R. Boccaccini, G. Ondracek, Prediction of the Poisson's ratio of porous materials, *J. Mater. Sci.* 31 (1996) 1643–1646.
- [14] K.D. Litasov, A. Shatskiy, P.N. Gavryushkin, I.S. Sharygin, P.I. Dorogokupets, A.M. Dymshits, E. Ohtani, Y. Higo, K. Funakoshi, P–V–T equation of state of siderite to 33 GPa and 1673 K, *Phys. Earth Planet. Inter.* 224 (2013) 83–87.
- [15] J. Zhang, I. Martinez, F. Guyot, R.J. Reeder, Effects of Mg-Fe<sup>2+</sup> substitution in calcite-structure carbonates: thermoelastic properties, *Am. Mineral.* 83 (1998) 280–287.
- [16] J.M. Moyer, G.S. Ansell, The volume expansion accompanying the martensite transformation in Iron–Carbon alloys, *Metall. Trans. A* 6 (1975) 1785–1791.
- [17] Z.C. Xia, J.W. Hutchinson, Crack patterns in thin films, *J. Mech. Phys. Solids* 48 (2000) 1107–1131.
- [18] H. Shi, W. Luo, B. Johansson, R. Ahuja, First-principles calculations of the electronic structure and pressure-induced magnetic transition in siderite FeCO<sub>3</sub>, *Phys. Rev. B* 78 (2008) 155119.
- [19] K. Gao, F. Yu, X. Pang, G. Zhang, L. Qiao, W. Chu, M. Lu, Mechanical properties of CO<sub>2</sub> corrosion product scales and their relationship to corrosion rates, *Corros. Sci.* 50 (2008) 2796–2803.
- [20] G. Schmitt, M. Mueller, M. Papenfuss, E. Strobel-Effertz, Understanding localized CO<sub>2</sub> corrosion of carbon steel from physical properties of iron carbonate scales, in: *Corrosion 99*, NACE International, Houston, TX, 1999, Paper No. 38.
- [21] F. Yu, K.W. Gao, Y.J. Su, J.X. Li, L.J. Qiao, W.Y. Chu, M.X. Lu, The fracture toughness of CO<sub>2</sub> corrosion scale in pipeline steel, *Mater. Lett.* 59 (2005) 1709–1713.
- [22] Y. Zhang, X. Pang, S. Qu, X. Li, K. Gao, The relationship between fracture toughness of CO<sub>2</sub> corrosion scale and corrosion rate of X65 pipeline steel under supercritical CO<sub>2</sub> condition, *Int. J. Greenhouse Gas Control* 5 (2011) 1643–1650.
- [23] S.D. Zhu, G.S. Zhou, J. Miao, R. Cai, J.F. Wei, Mechanical properties of CO<sub>2</sub> corrosion scale formed at different temperatures and their relationship to corrosion rate, *Corros. Eng., Sci. Technol.* 47 (2012) 177.
- [24] T. Nakamura, S.M. Kamath, Three-dimensional effects in thin film fracture mechanics, *Mech. Mater.* 13 (1992) 67–77.